CEA EURATOM

DRFC-SCP ÉUR-CEA-FC-1153

INTERNAL DISRUPTIONS IN TOKAMAKS : A TURBULENT INTERPRETATION

M.A. DUBOIS, A.L. PECQUET, C.REVERDIN

JUILLET 1982

INTERNAL DISRUPTIONS IN TOKAMAKS : A TURBULENT INTERPRETATION

M.A. DUBOIS, A.L. PECQUET, C. REVERDIN

ASSOCIATION EURATOM-CEA SUR LA FUSION
Département de Recherches sur la Fusion Contrôlée
Centre d'Etudes Nucléaires
Boîte Postale n°6. 92260 FONTENAY-AUX-ROSES (FRANCE)

ABSTRACT

High speed X-ray data of sawteeth in TFR are interpreted using a kinematic model. It is shown that the internal disruption begins for a small size of the q = 1 island, and that the sharp details observed on different chords are not reproduced by a total reconnection model. Conversely they are well simulated by a model where the temperature flattening is due to the propagation of a turbulent region starting from the q = 1 surface.

INTRODUCTION

It is more and more obvious that sawteeth are a very important mechanism to regulate the core of a tokamak discharge. Nevertheless there is no satisfiying theory of the internal q = 1 disruption : some evidence has already been given [1,2] of the inadequacy of the total reconnection model [3]. Other comparisons of this theory with X-ray data [4,5] did not find any contradiction, but they did not study the m = 1 mode behaviour, only the behaviour of poloidally averaged profiles (ie m = 0 phenomena). The kinematic model used in [1] to produce synthetic X-ray signals and therefore obtain the magnetic map as a function of time by a parameter fitting process showed that the m = 1 mode amplitude is well reproduced by a q = 1 island which stays fairly small up to the time of the disruption. But no precise mechanism for the disruption itself was incorporated, because the time resolution of the X-ray signals showed only a temperature drop in the center and a rise outside of the q = 1 surface. The new system of fast data acquisition and high performance amplifiers used on TFR soft X-ray array of surface barrier detectors often shows sharp spikes on a time scale shorter than the disruption itself. We have tried to incorporate disruption mechanisms in our kinematic model to compare then with the experimental data.

In the first paragraph we will point out the nature of the new phenomena observed. Then in § 2 we will give a phenomenological description of two possible disruption mechanisms. In paragraph 3 we will compare the synthetic signals with experimental data on several examples. We will then discuss the weaknesses of such a comparison and find out what conclusions can be drawn at this point and what further studies are needed. The technical details of the kinematic models will be given as an Appendix.

I) The m = 1 = 1 tearing island which develops on the q = 1 surface is responsible for the m = 1 mode observed on soft X-ray signals. We define three regions of plasma, the inner region or hot core which is the part of the plasma outside of the q = 1 island but inside the q = 1 surface, the island region, and the outer region, outside the island and outside the q = 1 surface. We also define the island width, δ island, the X and O points on fig 1. The usual behaviour during sawtooth activity is characterised by a regeneration part during which the temperature (and hence X - ray emissivity) profile becomes more and more peaked. An oscillation of m = 1 parity begins to grow until a point - the internal disruption - when the signal drops on the central traces due to a temperature flattening (fig 2). The kinematic model of Ref. [1] simulates this behaviour quite accuraly(fig 3) (fig 4) and even in this example where the m = 1 mode was very conspicious, the island was far from invading the whole plasma center (fig 5). Usually the amplitude of the m = 1 mode is much smaller and the island size at the onset of the disruption is only a small fraction of the radius of the q = 1 surface. Numerical values of interest for this case are given in table I.

In some cases, the disruption itself shows complicated signals : sharp spikes with no obvious phenomenological interpretation (fig 6). This is especially evident in low q ($q \lesssim 2,5$) high density ($ne \sim 2.10^{14} cm^{-3}$) discharges such as those used for neutral beam injection on TFR [16]. A parasitic origin for these spikes has been carefully ruled out. Moreover, such features seem to be present in all internal disruptions, but were not detected before because their amplitude relative to the m = 1 mode and to the total temperature variation was much less, and also because of the lesser time resolution of the experimental apparatus.

An accurate theory of the internal disruption should be able to predict these signals, that is a kinematic model the phenomenology of which would be based upon a correct theory of the disruption should yield synthetic signals exhibiting similar sharp features.

II) DESCRIPTION OF THE DISRUPTION MODELS

The description of the total reconnection model of the internal disruption is well known [3]. According to this theory, the m = 1 island invades the whole center of the discharge, and leaves flat temperature and current density profiles in the central region. As experimental data interpreted by the indirect cartography method of [1] show that the island size just before the disruption is still quite small, one is led to believe that if a total reconnection takes place, the internal disruption must consist of a tremendous acceleration of the m = 1 island growth rate. We have introduced this possibility into our kinematic model (see annex, § c), although there is no theoretical basis for it, as a last opportunity to reconcile the total reconnection model with the experiment.

Another possibility pointed out long ago [6] [7] is that the disruption is due to the onset of a fine grain turbulence which ergodizes flux lines, thus flattening the current density profile. The corresponding liberation of poloidal energy feeds the turbulence. This schema is also able to explain the q = 2 minor and major disruptions, the only difference being the cause of the turbulence onset : whereas it seems plausible that the nonlinear growth of tearing islands of different helicities can in same cases create, by overlapping a local ergodisation which developps in a self consistent turbulence [9] [10] there is no such possibility in q = 1 disruptions. Even for q = 2 disruptions, there are some cases where only the q = 2 island is present [11]. But it has been shown [8] that the linear evolution of a tearing island can lead to a catastrophic point - that is the evolution can no longer consist of a succession of quasi equilibria. This is also visible on numerical calculations of the evolution of the m = 1 island [12] [13] [14] [15] which for relevant values of s (s = resistive time: alfven time) reach a point where a singular current density layer appears at the X point - corresponding to the cancellation of the flux lines angle at the X-point of the separatrix, as shown in Ref. [8] - such a layer is unstable to high-m number resistive modes and a small turbulent region must appear in the vicinity of the separatrix. As shown in Ref. [6] and [7], such a turbulent region will propagate in the inner and outer regions, fed by the average current density gradient, ie the poloidal magnetic energy. The island itself will be left unchanged except perhaps if it is too small to survive a minute erosion at the separatrix. The turbulence propagation will continue as long as there is enough poloidal magnetic energy, and at most, when it reaches the center of the hot inner region, ie the displaced magnetic axis. Of course such a turbulence, consisting of a hierarchy of magnetic and kinetic eddies - enhances by a large factor the parpendicular heat conductivity, hence flattens the temperature across

the turbulent region. Then the resulting temperature (and hence emissivity) profile, is smoothed by normal heat conductivity. It is also possible that during the turbulent phase, the imperturbed magnetic structures - ie the remnant of the hot core and the m = 1 island - may have macroscopic motion and shape modification because the ergodized region around relaxes magnetic forces they experienced before. Such a possibility which is being studied theoretically has been kept open in our kinematic model : as we shall see it appears that in some cases there is indeed a move of the hot core away from the X point.

III) COMPARISON OF SYNTHETIC SIGNALS WITH EXPERIMENTAL DATA

The first example is an internal disruption during neutral beam injection. Fig 8 shows the experimental signals : one can distinguish the m = 1 precursor, then a fast complex phenomenon occuring without measurable time lag on all the chanels, and lastly a rather slow smoothing of the signals, which corresponds to a normal heat conduction process after the catastrophic part of the disruption. Fig 9a shows synthetic signals obtained with a total reconnection process. The island growth rate has been enhanced by a factor of 100 at the onset of the disruption. Nevertheless the fit is not very good mainly because the disruption is too slow. If one tries to further enhance the growth rate, the behaviour of the synthetic signals is even more different to the experiments (for instance at r = 3,7 cm a large negative spike replace the small positive one, etc.). Fig 9b shows synthetic signals obtained with the turbulent model. The general behaviour is remarkably similar to the experimental data (especially if one is reminded that we do not introduce a real heat conductivity in our simple model, hence a too rapid smoothing of the signal after the catastrophic event on the outer channels - see appendix). Fig 10 shows the radial amplitude of the sawtooth compared to the total signal for experimental and calculated signals. Here also the agrement is very good showing that the hypothesis on the emissivity profiles in the kinematic model are correct. Fig 12 a shows the island at the onset of the disruption and fig 12b the situation at the end of the disruptive period. The turbulence does not reach the center. The central core has moved toward the O-point. There is no experimental evidence that the m = 1 island is still in existence. Fig 11 shows the time evolution of the emissivity profiles during the disruption. Numerical values (for this case are given table II. Fig 13 shows another example of internal disruption in slightly different conditions. The signals during the disruption are markedly different, which is to a large extant due to a different phase relation between the m = 1 island and the detectors. We were unable to simulate -even grossly - this behaviour with a total reconnection model, whereas fig 14 shows that the turbulent model gives a very good result. Fig 15 shows the time evolution of the emissivity profiles and fig 16 the magnetic configuration at the beginning (16a) and at the end (16b) of the turbulent phenomenon. The hot core has not moved much in this case. Quantitative values for this case are given in table III.
The next example is of an ohmic discharge (without additional heating), fig 17-18. The island width at the onset of the disruption is even smaller ($\sim$ 7 mm) as in the two preceding cases (fig 19). If we compare this with the first case studied (fig 2 to 5) and with the two examples given in ref. [1], it seems that the

critical isalnd width (ie the isalnd width at the onset of the disruption, which, according to ref [8] is the island size at which the angle at the X-point of the separatrix cancels) depends of the radius of the q = 1 surface, namely, that the disruption appears for smaller island size when the q = 1 radius r_o is large than when it is small. numerical values for this case are given in table IV. It sometimes happens that the beaviour is more complex : fig 20 shows experimental signals in an ohmic discharge where a very large m = 1 activity follows the disruption. Using our experience with more classical cases we can give a tentative explanation : at time t_1 turbulence sets in followed by a displacement of the hot core towards the 0 point of the island. After this turbulent period the magnetic structure presents a stongly eccentric hot core. Then at time t_2 a new turbulent episode sets in which brings back the hot core to a less eccentric position. The two successive bursts of turbulence are clearly indicated by the temperature rises on external traces at plus and minus 9.4 cm.

IV) CONCLUSION

It must be clear that we do not pretend to have a physical simulation of the sawtooth : we use a kinematic model based on a phenomenology inspired by analytical results, and compare the synthetic signals to the actual data. The size of the q = 1 island at the onset of the disruption is firmly established to be smaller than q = 1 radius. As for the mechanism of the disruption itself, it seems that the total reconnection model is incompatible with the data, whereas the experimental signals are well reconstructed by a turbulent disruption scheam in which a turbulent region appears and propagates from the separatrix. In the extensive data which we have examined, this turbulence always seems to stop before reaching the magnetic axis, thus leaving a hot central core the temperature of which drops by thermal conductivity. In some cases mainly during the very large sawteeth observed during neutral beam injection, but also in a few ohmic heating discharges, the very small q = 1 island present at the disruption onset seems to be destroyed by the turbulence, a fact which is made apparent by the movement of the hot core towards the O-point of the island during the turbulent phase. The dependance of the island size at the onset of the turbulence, on the radius of the q = 1 surface very probably means that the angle at the X-point of the separatrix is a function of the temperature and density gradients. For small enough values of the gradients ie when the q = 1 radius is small or when additional heating broadens the temperature and density profiles, the island is probably able to reach a large width without reaching its catastrophic point, and then the sawtooth is dominated by the large m=1 mode as in the helium discharge studied above. The enhanced transport due to the large m = 1 island may even be sufficient to regulate the central region and prevent temperature peaking. The sawtooth would then disappear completely as observed for instance on ISX-B [17]. A precise analytical study of the separatrix angle as a function of the temperature and density gradients is necessary to understand all possible types of behaviour. On the other hand, a more complete theoretical analysis turbulence during the disruption itself is being completed [18]. Experimental confirmation (or denial) of the turbulent model can be sought by measuring locally the turbulence during the disruption (which needs a high spatial and temporal resolution temperature diagnostic) and by extendring to other tokamaks the preceeding method. Pathological cases, for instance during impurity injection, can also give useful clues.

Aknowledgments :

It is a pleasure to thank Drs A. Samain D. Marty, and L. Laurent for useful discussions, and the TFR computer team for valuable help.

ANNEX

DESCRIPTION OF THE KINEMATIC MODEL AND THE INTRODUCTION OF A PROPAGATING TURBULENT REGION

The kinematic model used in [1] to produce synthetic X-ray signals mapped the magnetic surfaces in presence of the island with the polar equations [Fig. 1]

$$(1)\quad \begin{aligned} p_1(\theta,\xi) &= \delta\cos\theta + (r_o^2-\delta^2\sin^2\theta)^{1/2} - \delta_1(\cos^2\tfrac{\theta}{2} + \xi - 1) \text{ inside the unperturbed } q=1 \text{ surface} \\ p_2(\theta,\xi) &= \delta\cos\theta + (r_o^2-\delta^2\sin^2\theta)^{1/2} + \delta_2(\cos^2\tfrac{\theta}{2} + \xi - 1) \text{ outside} \end{aligned}$$

with :

$\delta_1 + \delta_2 = \delta_{isl}$ (δ_{isl} is the island width)

$\delta_2 = \mathcal{A}\, S_1$ $\mathcal{A}$ determines the asymmetry of the island ($\mathcal{A} = 0.9$ see [8])

$\delta = \mathcal{C}\,\frac{S_1}{2}$ δ gives the displacement of the hot core toward the X point during the island growth ($\mathcal{C} = 0.7$ usually)

ξ labels a magnetic surface.

The X-ray emissivity in each point is then given by

$$(2)\quad \phi(\zeta) = \phi_o\,\frac{\exp - p(\zeta/a)^2}{\exp - p(r_1/a)^2}$$

where : $\zeta = p_1(\Pi,\xi)$ for inner surface

$\zeta = p_2(\Pi,\xi)$ for outer surface

$\zeta = r_o - \delta$ inside the island

a the limiter radius

r_1 the temperature inversion radius

p the peaking parameter

It means that as measured experimentally the X-ray emissivity profile without island is usually gaussian (the cases where there is a large influx of impurities are not studied here). The whole emissive structure is then rotated at the mode frequency and the chord integrated X-ray signals are synthesized taking into account the geometry of the experimental apparatus. The phenomenology and the time behaviour of the different parameters are described on Figure 7b.

a) The regeneration part of the sawtooth

During the regeneration part of the sawtooth the peaking parameter grows with the empirical law :

(3) $p = p_o \left[1 + \frac{1}{\alpha} \left(\frac{t}{\tau_p} \right)^{\alpha} \right]$ where t is the time since the preceeding disruption p_o is the value of p just after disruption, α of order 1 and τ_p a characteristic time of the order of the sawtooth period. When the value p_1 is reached the island begins to grow. The time evolution of the island width δ_{isl} used, is the analytical law found in [8] and is given by

(4a) $$\frac{d(\delta_{isl})^2}{dt} = K \frac{a^2}{\tau_{isl}} \quad \text{where} \quad \begin{cases} K = p - p_1 & \text{if } \delta_{isl} \geq \delta_{min} \\ K = 0 & \text{if } \delta_{isl} < \delta_{min} \end{cases}$$

a is the limiter radius, τ_{isl} the characteristic time of the island growth, δ_{min} the minimum width of the island.

The island grows until it reaches the critical size δ_{crit}. Then the disruption phase starts again. In reference [1] , the disruption was simulated by a mere decrease of the peaking parameter, and no physical mechanism was suggested for this temperature flattening :

(5) $\frac{dp}{dt} = -\frac{k}{\tau_p} p$ where k is the ratio of the regeneration time to the disruption duration.

In the simulation of the reference [1] , during both the regeneration and the disruption, the emissivity in each point was given by equation (2).

b) The turbulent mechanism for the disruption

In order to simulate the sharp features that the very fast data acquisition has shown, we incorporated the turbulent mechanism in the simulation. As described in § II, the turbulence starts in the vicinity of the separatrix. During this phase the inner radial extension r_{int} of the turbulent region propagates with the law

(6a) $r_{int} = (r_o - \delta) \frac{t_1}{\tau_{tur}} \mathcal{R}_{tur}$ for $t_1 \leq \tau_{tur}$

where $\mathcal{R}_{tur}$ defines the maximum extension of the turbulent region
τ_{tur} is the turbulence phase duration

t_1 is the time since the turbulence onset.

At the same time the outer extension is given by

(6b) $$r_{out} = r_{int} \times \mathcal{A}_{tur} \quad \text{for } t_1 \leq \tau_{tur}$$

where $\mathcal{A}_{tur}$ determines the asymmetry of the turbulence.

We have also been led to introduce the possibility of a motion along OX of the hot core during the disruption compared to its position at the end of the disruption. It is assumed by :

(7a) $$X = X_{tur} \times \frac{t_1}{\tau_{tur}} \quad \text{if } t \leq \tau_{tur}$$

and

(7b) $$X = X_{tur} \left\{ 1 - \frac{t_1 - \tau_{tur}}{\tau_{dis} - \tau_{tur}} \right\} \quad \text{if } t > \tau_{tur}.$$

Equation 7b yields the return motion of the hot core toward its initial position at the beginning of the new sawtooth. X_{tur} determines the maximum displacement of the hot core and is an adjustable parameter. τ_{dis} is the duration of the disruption i.e. the time needed by the peaking parameter to decrease until reaching initial value p_o.

During the turbulent phase the island stays arbitrarily at its maximum size δ_{crit}. It decreases for $t_1 > \tau_{tur}$ with the following law :

(4b) $$\delta_{isl} = \mathcal{H} \delta_{crit} \left(1 - \frac{t_1 - \tau_{tur}}{\tau_{id}} \right)$$

where $\mathcal{H} = 0$ if $\delta_{isl} \leq \delta_{min}$
$= 1$ if $\delta_{isl} > \delta_{min}$

τ_{id} is an ajustable parameter and is the island decrease time constant.

In order to compute the local emissivity for $t_1 \leq \tau_{tur}$ the plane is divided as before in three regions :

- The turbulent region : its emissivity is taken equal to the island one to assume the temperature flattening. The X-ray emissivity in each point is then given by (2) with $\zeta = r_o - \delta$

- The outward region : the X-ray emissivity in each point is given by (2) with $\zeta = p_2(\Pi,\xi)$
- The inner region : it is the same local function $\phi(\zeta)$ with $\zeta = p_1\{\Pi,\xi(X)\}$ to take into account the hot core motion along OX.

For $\tau_{tur} < t_1 \leq \tau_{dis}$, i.e. the end of the internal disruption, the local emissivity is calculated as follows :

$$\phi(\zeta) = \phi_1(\zeta)\,\frac{t_1 - \tau_{tur}}{\tau_{dis} - \tau_{tur}} + \phi_2(\zeta)\,\frac{\tau_{dis} - t_1}{\tau_{dis} - \tau_{tur}}$$

where $\phi_1(\zeta)$ is a profile without turbulence (i.e. $r_{int} = r_{out} = X = 0$)
$\phi_2(\zeta)$ is the profile with maximum extension turbulence.

This averaging is introduced to simulate the effect of thermal conductivity the real introduction of which would be too expensive in computer time. But because it is simultaneous across the whole profile, if one adjusts correctly the time constant of this process near the plasma center, it will appear too fast on the outer traces, which explains a large number of the imperfections in the simulation. Figures 11 and 15 show the evolution of profiles during the disruption : the former exhibits an horizontal displacement of the hot core, the latter does not.

c) Total reconnexion modal

To simulate the total reconnexion theory of internal disruption, one needs a law for the non linear growth rate. As it has been shown that, up to the time of the disruption, the analytical law given in [8] was satisfying and that at this time the island size was rather small, it is necessary to introduce a much more rapid evolution during the disruption. It is done by suddenly dividing the characteristic time τ_{isl} by an adjustable parameter η, then the island evolves until the disappearance of the hot core. During this phase, the local emissivity is given by

$$A(\zeta) = \frac{\delta_{isl} - \delta_{max}}{\delta_{crit} - \delta_{max}}\,\phi_1(\zeta) + \frac{\delta_{crit} - \delta_{isl}}{\delta_{crit} - \delta_{max}}\,\phi_2(\zeta)$$

where ζ is defined as in (2)
δ_{isl} is the island size
δ_{max} is the island size when it invades the total $q = 1$ surface
δ_{crit} is the island size at the disruption time

$\phi_1(\zeta)$ is the local emissivity function as defined in (2) with δ_{isl} and p calculated parameters

$\phi_2(\zeta)$ is the local emissivity function as defined in (2) but without island and with p_o peaking parameter. It is the local emissivity function at the beginning of the new sawtooth.

The best results are obtained with value of $\eta \sim 100$, smaller values leading to a much too slow behavour during the disruption, and higher values leading to sharp features with systematically uncorrect phases compared to the experimental signals.

d) Methodological remark

We have tried to keep the kinematic model as simple as possible to avoid the introducing of too many parameters. All the parameters we used are directly measured on the experimental data or come from theory except :

- for the predisruptive phase :
  - . the q = 1 radius
  - . the temperature inversion radius
  - . the critical island size

- for the disruptive phase :
  - . the maximum extent of the turbulence
  - . the turbulence asymetry
  - . the displacement of the hot core
  - . the turbulence propagation speed

As our kinematic model is mainly an indirect cartography method, it is not surprising that we have to adjust by trial and error these quantities which are precisly those that we wish to know. The same wish for simplicity precluded the introduction of thermal conductivity, impurity transport, etc... as we were mainly concerned by the MHD behaviour.

BIBLIOGRAPHY

[1] Dubois, M.A., Marty, D., Pochelon, A. : Nuclear Fusion 20 1355 (1980).

[2] Saufhoff, N. : proceedings of the IAEA Symposium on disruptions, Garching 1979

Eames, D. : Ph.D. thesis (Princeton University, 1981).

[3] Kadomtsev, B.B. : Fiz Plazmy 1 (1975) 710.

[4] Jahns, G.L., Solar, M., Waddell, B.V., Callen, J.D., Hicks, H.R. : Nuclear Fusion 18, 609 (1978).

[5] Yamamoto, S. : Nuclear Fusion 21, 992 (1981)

[6] Samain, A. : Plasma Phys. 18 (1976) 551.

[7] Dubois, M.A., Samain, A. : in Plasma Physics and Controlled Nuclear Fusion Research (Proc. 7th Int. Conf. Innsbruck, 1978) Vol. 1, IAEA, Vienna (1979) 615.

[8] Dubois, M.A., Samain, A. : Nuclear Fusion 20, 1101 (1980).

[9] Carreras, B.proceedings of the 1981 Sherwood Meeting.

[10] T.F.R. Group : "Disruptions in T.F.R. 600" report EUR-CEA 1151.

[11] T.F.R. Group : Nuclear Fusion 18, 647 (1978).

[12] White, R.B., Monticello, D.A., Rosenbluth, M.N., Waddelle, B.V. : in PP & CNFR (Proc. 6th Int. Conf., Berchtesgaden, 1976) Vol. 1, IAEA Vienna (1977) 569.

[13] Carreras, B. and al : proceedings of the IAEA Symposium on disruptions, Garching 1979.

[14] White, R.B. : private communication.

[15] Carreras, B. : private communication.

[16] T.F.R. Group : in P.P. and CNFR (Proc. 8th Int. Conf., Bruxelles 1980) Vol. 1, IAEA, Vienna (1981).

[17] Hogan, J. : (ISX-B) private communication.

[18] Samain, A., Dubois, M.A. : to be published.

Nature of the gas		$D_2 + H_e$
Plasma current	I_p	200 kA
Toroidal field	B	40 kG
Central electronic density	n_e	$1.0 \times 10^{14}/cm^3$
Electronic temperature	T_e	1050 eV
Limiter radius	a	20 cm
Horizontal displacement	ΔR	2 cm
Sawtooth duration		3.2 ms
Mode frequency	f	7 kHz
Slowing parameter		0.4
Minimum value of peaking parameter	p_o	8
Maximum value of peaking parameter		10
Critical value of peaking parameter	p_1	9.5
Characteristic time of ohmic peaking	τ_p	10.3 ms
Geometrical coefficients	$\mathscr{C}$	0.5
	$\mathscr{A}$	0.9
Temperature inversion radius	r_1	6 cm
Radius of q = 1 unperturbed surface	r_o	5.1 cm
Characteristic time of island growth	τ_{isl}	15 µs
Minimum island width	δ_{min}	0.25 cm
Island width at disruption	δ_{crit}	3.7 cm

- Table I -

Plasma current	I_p	300 kA
Toroidal field	B_T	40 kG
Central electronic density	n_e	$1.7 \times 10^{14}/cm^3$
Electronic temperature	T_e	1.2 keV
Limiter radius	a	20 cm
Horizontal displacement	ΔH	2.5 cm
Sawtooth duration		8 ms
Mode frequency	f	3.5 kHz
Slowing parameter		0.7
Minimum value of peaking parameter	p_o	3.9
Critical value of peaking parameter	p_1	6.2
Characteristic time of island growth	τ_{isl}	70 μs
Minimum island width	δ_{min}	~ 0 cm
Island width at the disruption	δ_{crit}	1.05 cm
Turbulent phase duration	τ_{tur}	30 μs
Inner radial extension coefficient of the turbulence	$\mathcal{R}_{tur}$	0.3
Turbulent asymmetry	$\mathcal{A}_{tur}$	0.6
Displacement of the hot core	X_{tur}	2.5 cm
Island decay time	τ_{id}	200 μs
Characteristic time of ohmic peaking	τ_p	12.3 ms
Temperature inversion radius	r_1	8.34 cm
Radius of q = 1 unperturbed surface	r_o	7.25 cm

- Table II -

Plasma current	I_p	300 kA
Toroidal field	B_T	40 kG
Central electronic density	n_e	$1.7 \times 10^{14}/cm^3$
Electronic temperature	T_e	1.2 keV
Limiter radius	a	20 cm
Horizontal displacement	ΔH	2.5 cm
Sawtooth duration		8 ms
Mode frequency	f	3.5 kHz
Slowing parameter		0.5
Minimum value of peaking parameter	p_o	3.8
Critical value of peaking parameter	p_1	6.5
Characteristic time of ohmic peaking	τ_p	10.2 ms
Temperature inversion radius	r_1	7.9 cm
Radius of q = 1 unperturbed surface	r_o	7.2 cm
Characteristic time of island growth	τ_{isl}	24 μs
Minimum island width	δ_{min}	~ 0 cm
Island width at the disruption	δ_{crit}	1.05 cm
Turbulent phase duration	τ_{tur}	30 μs
Inner radial extension coefficient of turbulent	R_{tur}	0.45
Turbulence asymmetry	$\mathcal{A}_{tur}$	0.5
Displacement of the hot core	Σ_{tur}	0 cm
Island decay time	τ_{fd}	200 μs

- Table III -

Plasma current	I_p	300 kA
Toroidal field	B_T	40 kG
Central electronic density	n_e	$1.7 \times 10^{14}/cm^3$
Electronic temperature	T_e	1.3 keV
Limiter radius	a	20 cm
Horizontal displacement	ΔH	2 cm
Sawtooth duration		3.15 ms
Mode frequency	f	3.5 kHz
Slowing parameter		0
Minimum value of peaking parameter	p_o	3.8
Critical value of peaking parameter	p_1	5.8
Characteristic time of ohmic peaking	τ_p	5 ms
Temperature inversion radius	r_1	8.6 cm
Radius of q = 1 unperturbed surface	r_o	7.8 cm
Characteristic time of island growth	τ_{isl}	30 µs
Minimum island width	δ_{min}	$\sim$ 0 cm
Island width at the disruption	δ_{crit}	0.7 cm
Turbulent phase duration	τ_{tur}	30 µs
Inner radial extension coefficient of turbulence	R_{tur}	0.3
Turbulence asymmetry	Λ_{tur}	0.3
Displacement of the hot core	X_{tur}	1.5 cm
Island decay time	τ_{id}	50 µs

- Table IV -

FIGURE CAPTIONS

Fig. 1 Geometry of the magnetic surfaces.

Fig. 2 Example 1 - Soft X-ray signals at different radii during an helium discharge.

Fig. 3 Example 1 - Synthetic signals obtained by the simulation.

Fig. 4 Example 1 - Comparison between experimental and synthetic profiles of $\frac{\Delta A}{A}$, the ratio of the sawtooth amplitude to the main signal.

Fig. 5 Magnetic map at the disruption.

Fig. 6 Soft X-ray signals at different radii showing an ohmic turbulent discharge.

Fig. 7a Geometry of the turbulent region.

Fig. 7b Phenomenological description of the simulation code.

Fig. 8 Example 2 - Soft X-ray internal disruption at different radii during a discharge with neutral beam injection (100 μs/div.).

Fig. 9a Example 2 - Synthetic signals obtained with the total reconnexion model (100 μs/div.).

Fig. 9b Example 2 - Synthetic signals obtained with the turbulent model (100 μs/div.).

Fig. 10 Example 2 - Comparison between experimental and synthetic profiles of $\frac{\Delta A}{A}$.

Fig. 11 Example 2 - Emissivity function during the internal disruption.

Fig. 12 Example 2 - a - Magnetic map at the disruption onset.
b - Magnetic map at the end of the turbulent phase.
(The island in in black, the turbulent region in white).

Fig. 13 Example 3 - Soft X-ray internal disruption at different radii during a discharge with neutral beam injection (100 μs/div.).

Fig. 14 Example 3 - Synthetic signals obtained with the turbulent model (100 μs/div.).

Fig. 15 Example 3 - Emissivity functions during the internal disruption.

Fig. 16 Example 3 - a - Magnetic map at the disruption onset.
b - Magnetic map at the end of the turbulent phase.

Fig. 17 Example 4 - Soft X-ray internal disruption (the same as Fig. 6) during an ohmic discharge (100 μs/div.).

Fig. 18 Example 4 - Synthetic signals obtained with the turbulent model (100 μs/div.).

Fig. 19 Example 4 - a - Magnetic map at the disruption onset.
b - Magnetic map at the end of the turbulent phase
c - Magnetic map at the end of the disruption, after turbulent phase.

Fig. 20 Soft X-ray sawtooth showing a "pathological" internal disruption.

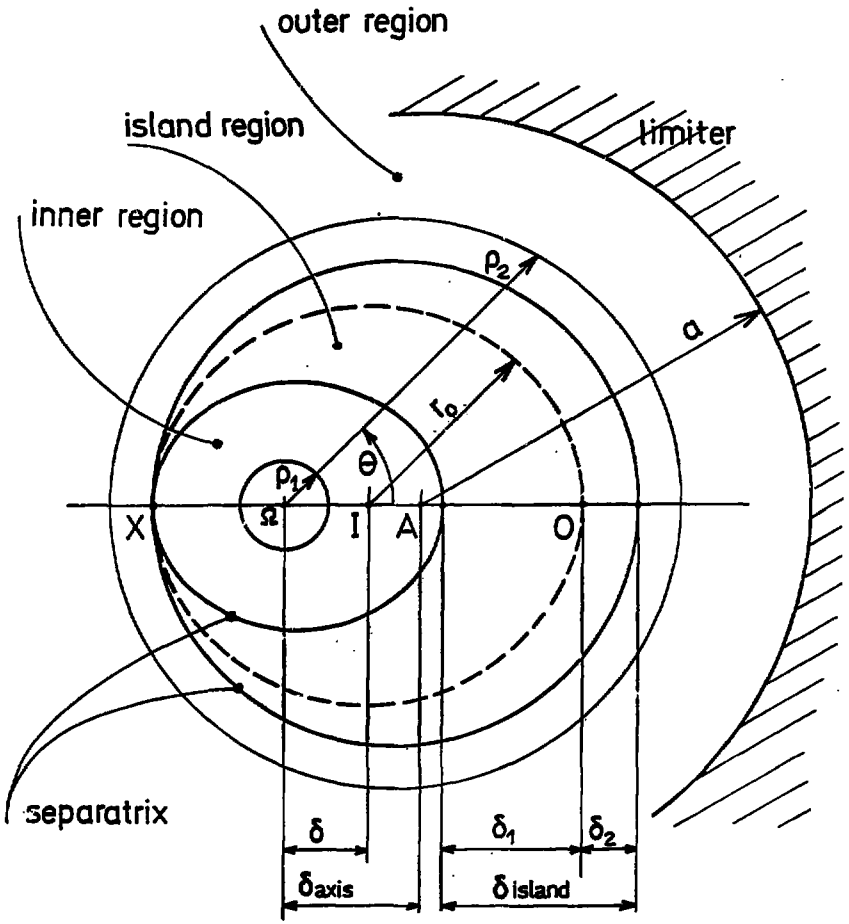
outer region
island region
inner region
limiter
separatrix
ρ_2
a
r_o
ρ_1
θ
X
Ω
I
A
O
δ
δ_1
δ_2
δ_{axis}
δ_{island}

Fig. 1

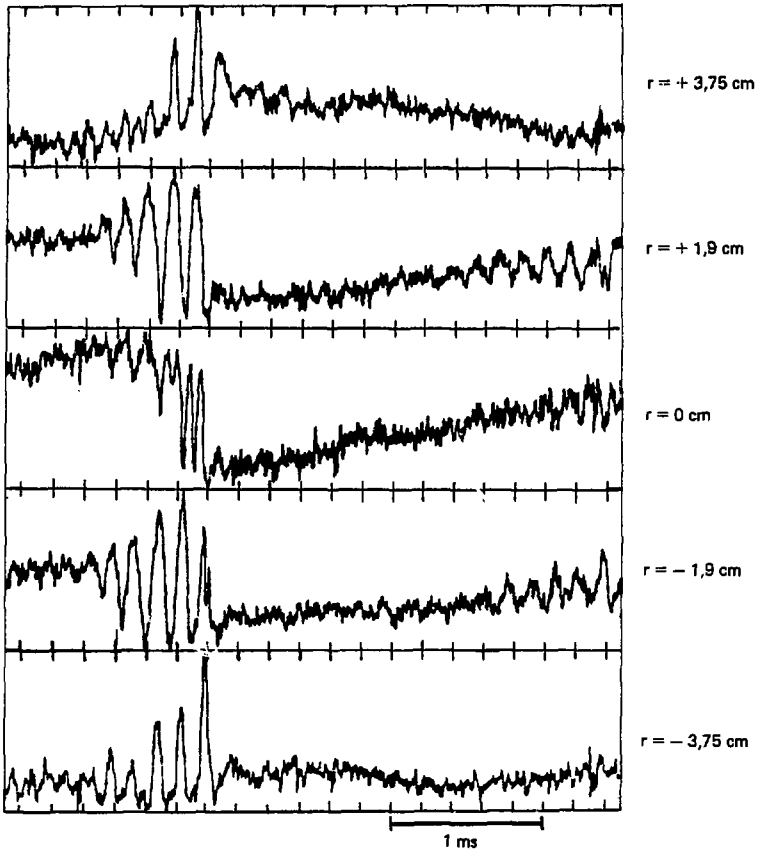

FIG. 2

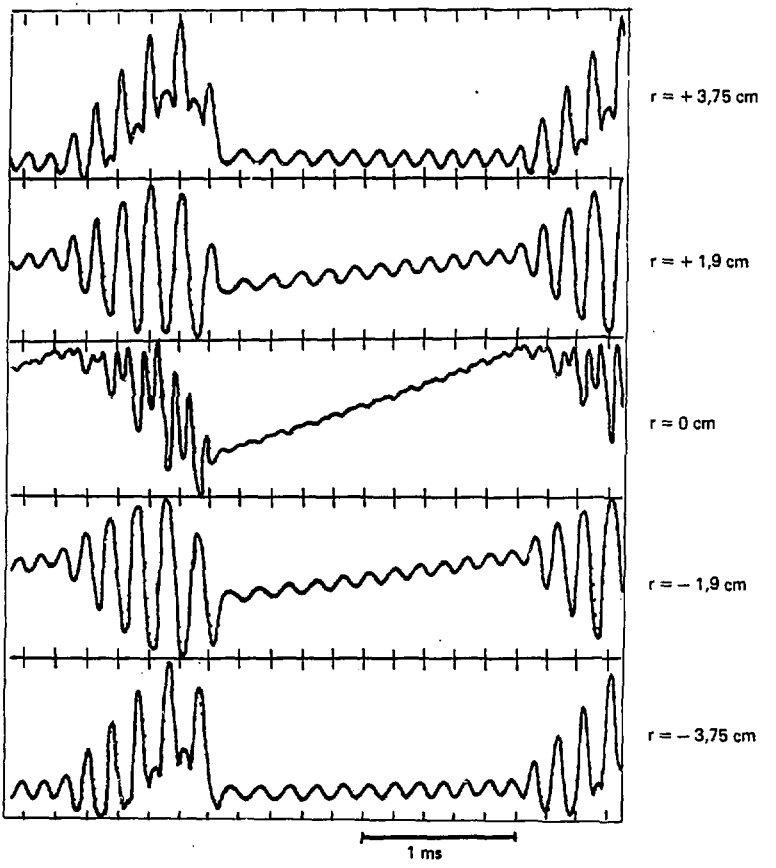

FIG. 3

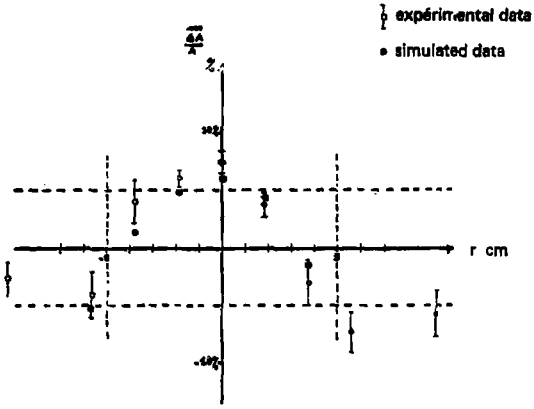

FIG. 4

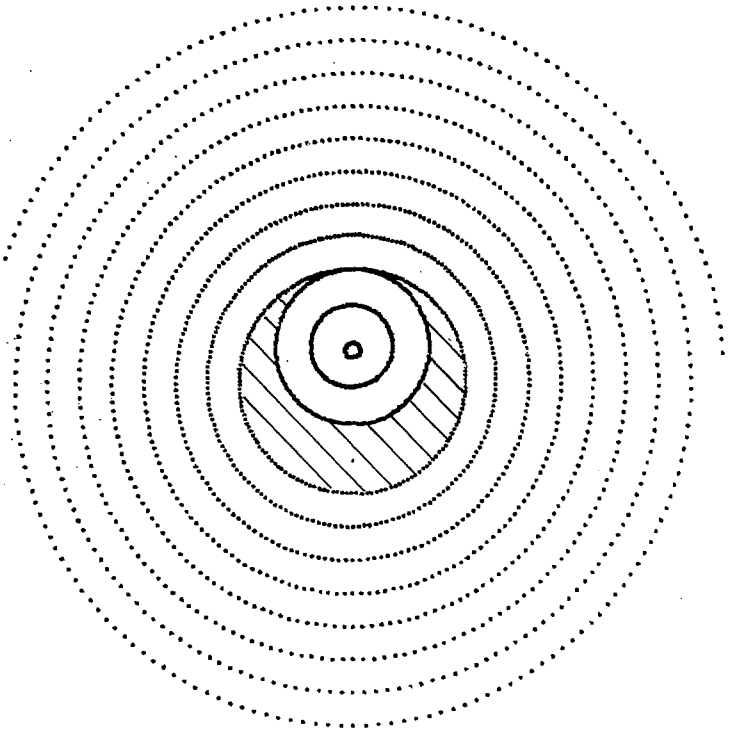

FIG. 5

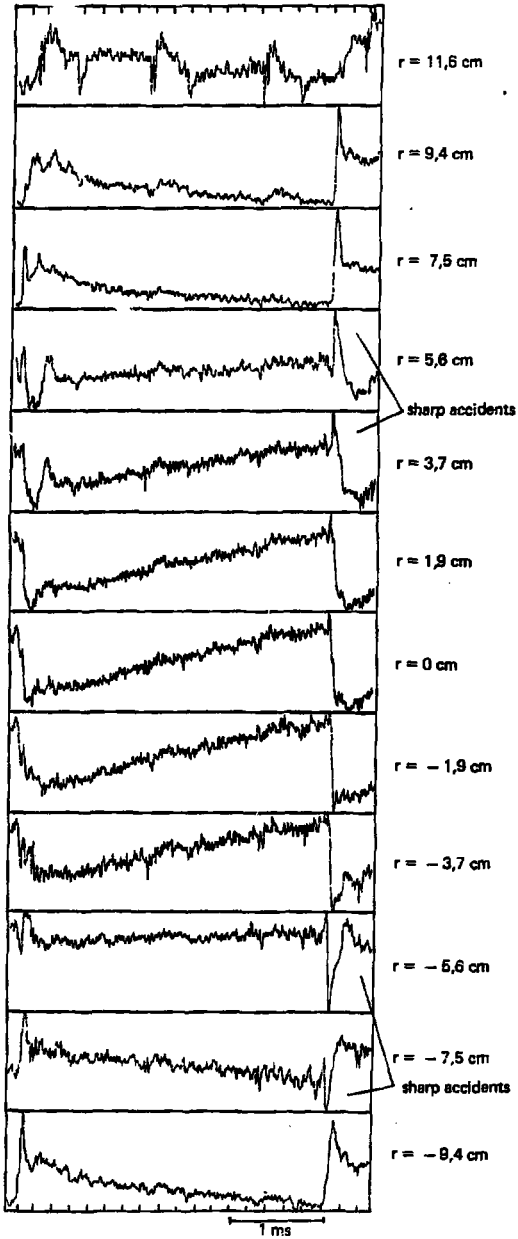
r = 11,6 cm
r = 9,4 cm
r = 7,5 cm
r = 5,6 cm
sharp accidents
r = 3,7 cm
r = 1,9 cm
r = 0 cm
r = − 1,9 cm
r = − 3,7 cm
r = − 5,6 cm
r = − 7,5 cm
sharp accidents
r = − 9,4 cm
1 ms

FIG. 6

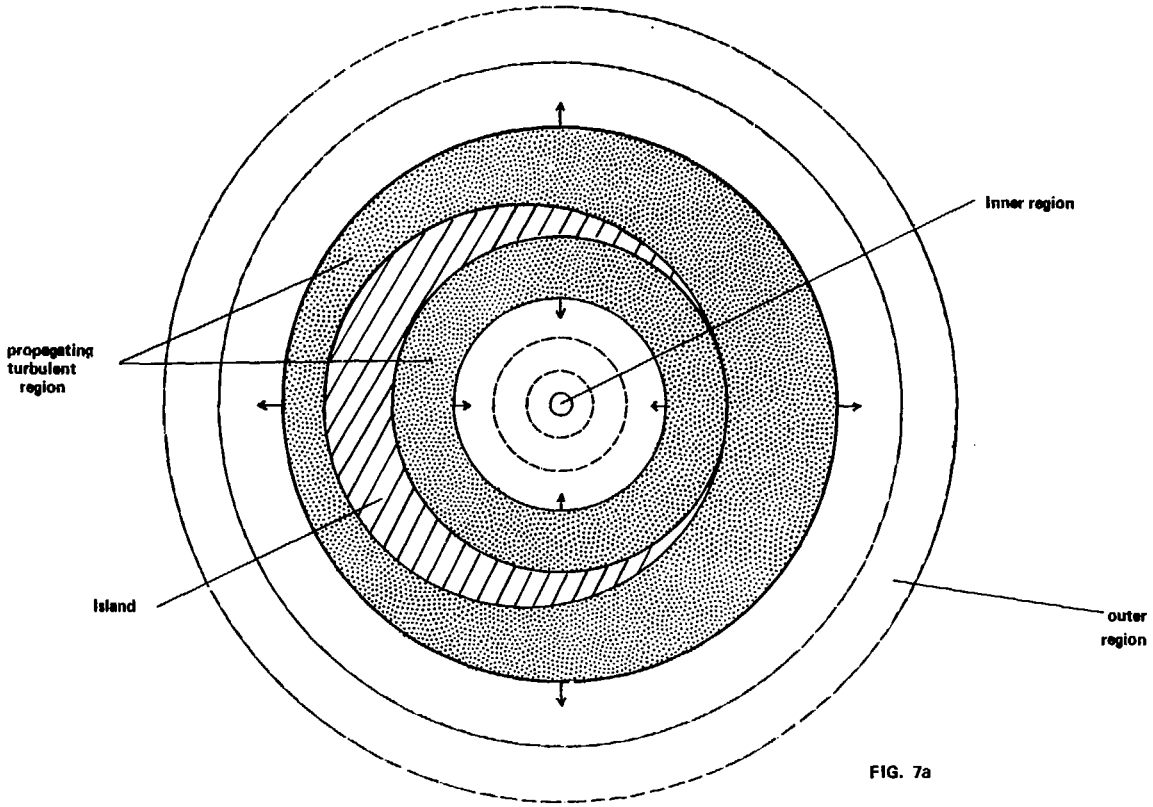
Inner region
propagating
turbulent
region
Island
outer
region

FIG. 7a

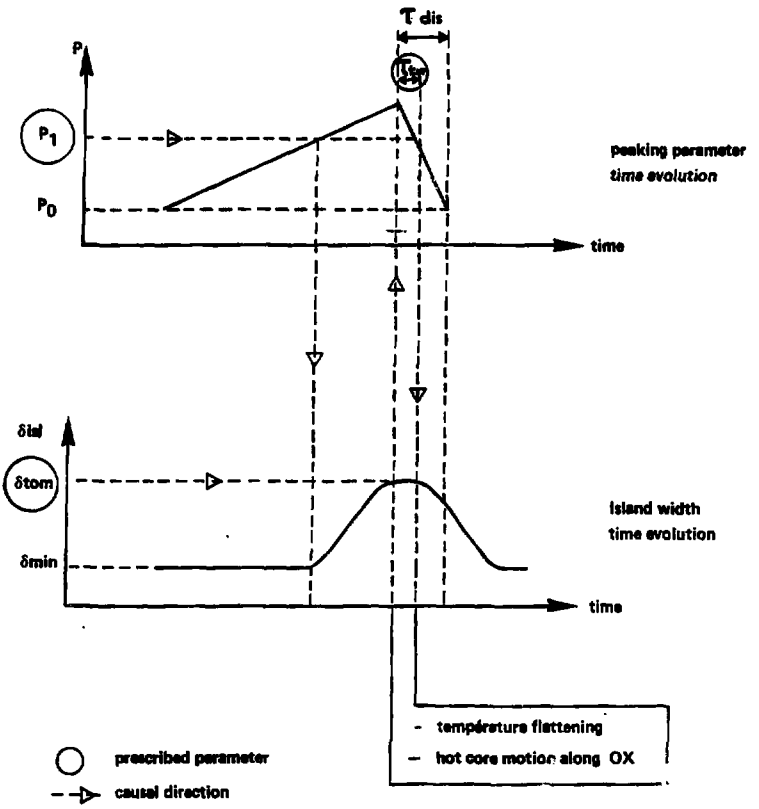
τ dis
P
P1
P0
peaking parameter
time evolution
time
δisl
δtom
δmin
island width
time evolution
time
- temperature flattening
- hot core motion along OX
prescribed parameter
causal direction

FIG 7b

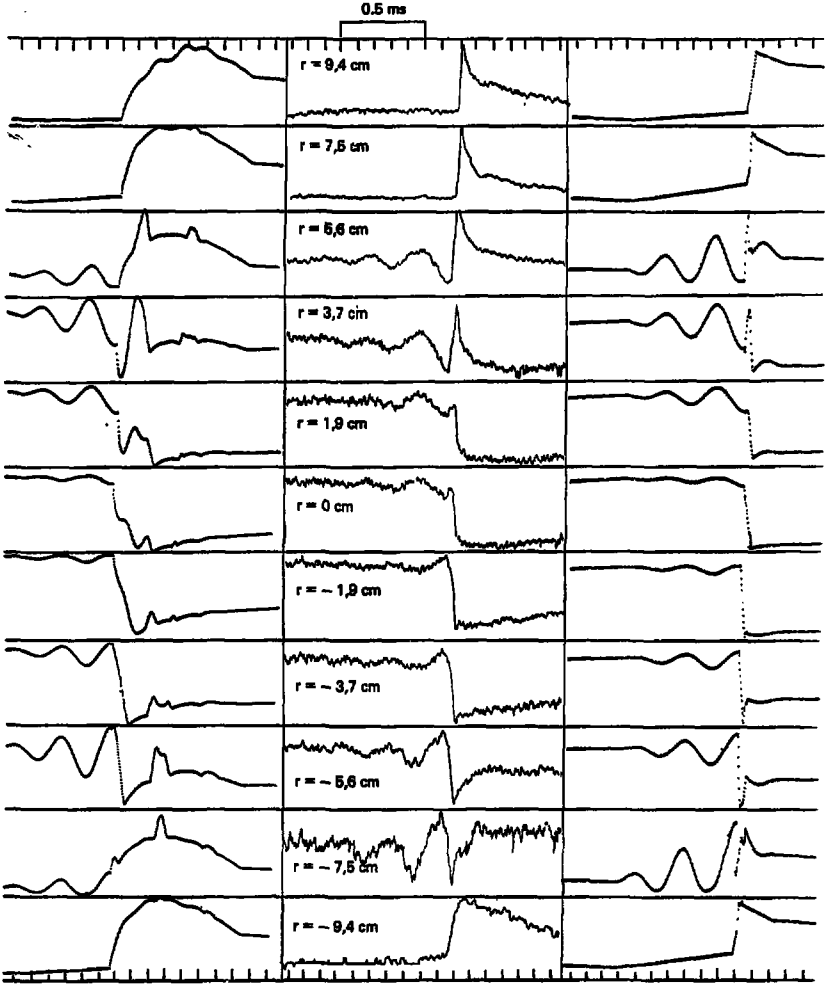

FIG. 9a FIG. 8 FIG. 9b

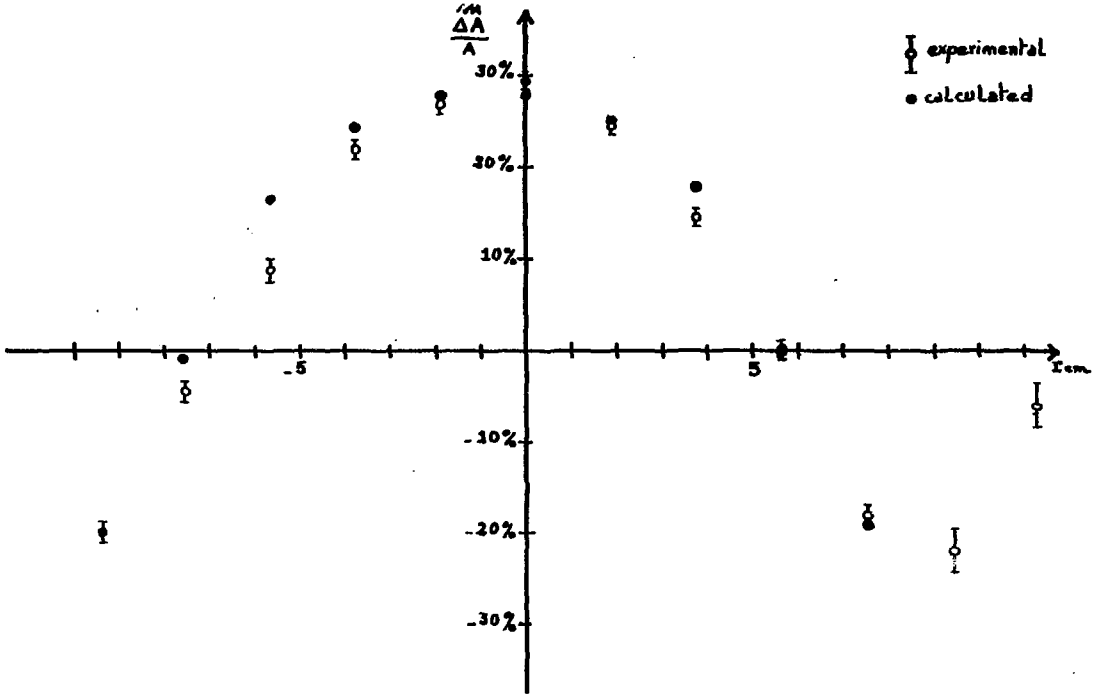

- Fig 10 -

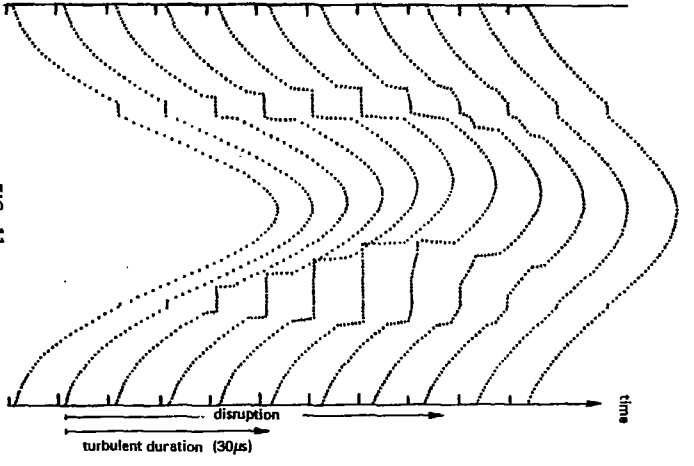

FIG. 11

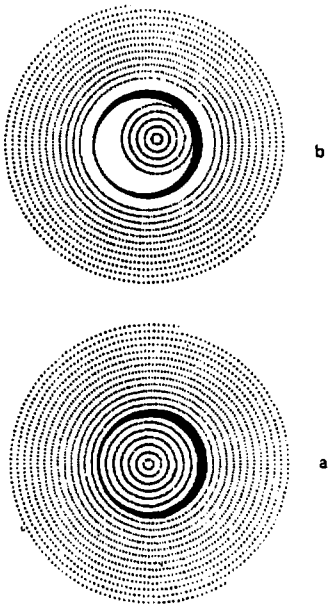

FIG. 12

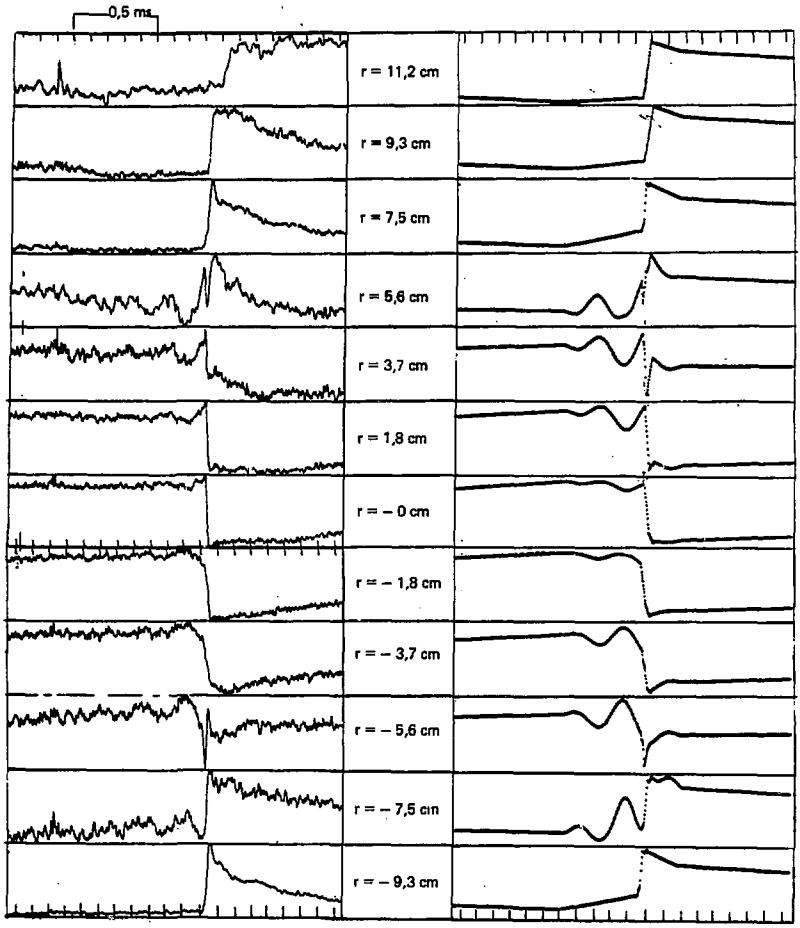
0,5 ms
r = 11,2 cm
r = 9,3 cm
r = 7,5 cm
r = 5,6 cm
r = 3,7 cm
r = 1,8 cm
r = – 0 cm
r = – 1,8 cm
r = – 3,7 cm
r = – 5,6 cm
r = – 7,5 cm
r = – 9,3 cm

FIG. 13

FIG. 14

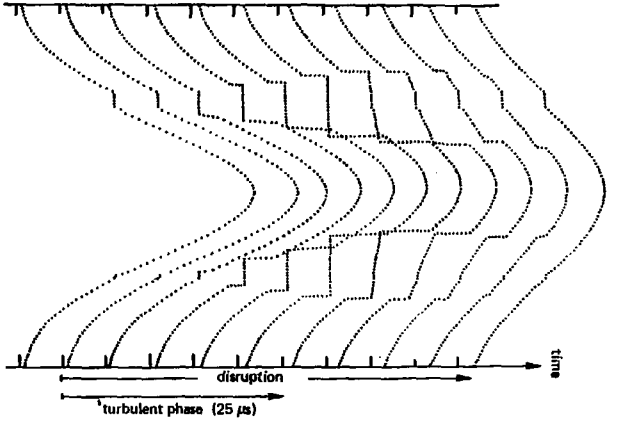

FIG. 15

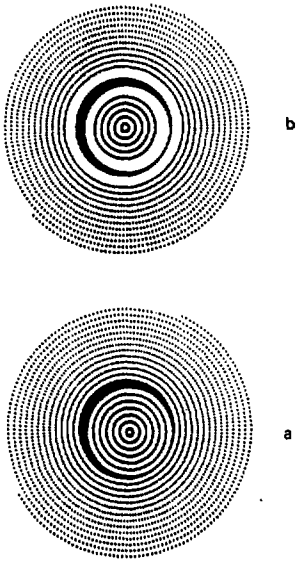

FIG. 16

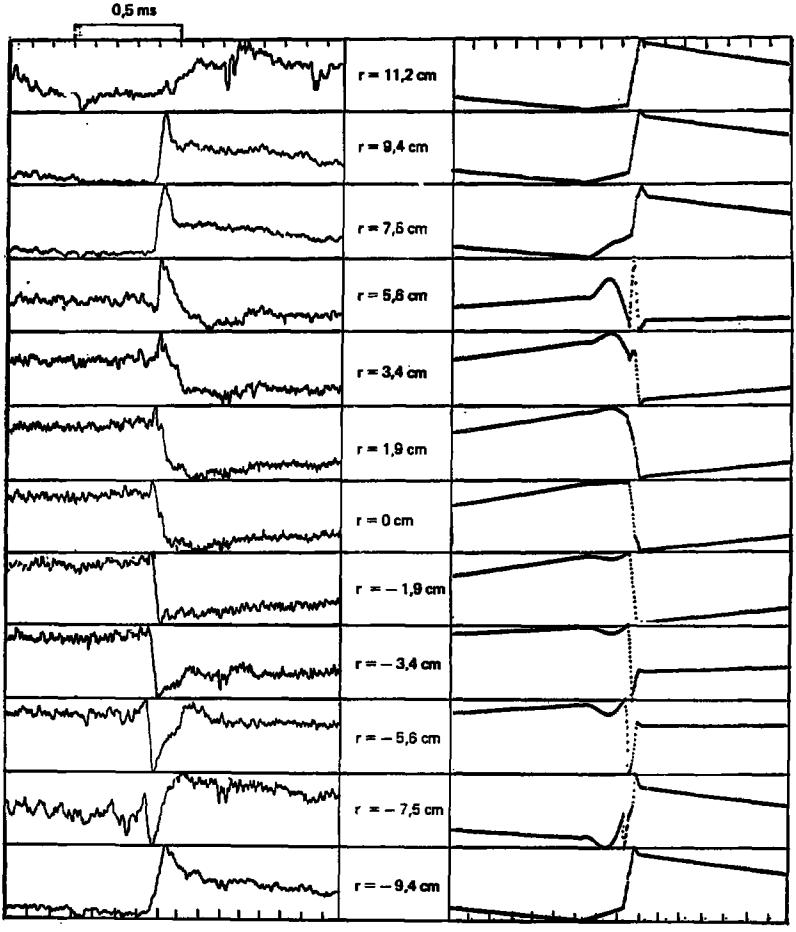
0,5 ms
r = 11,2 cm
r = 9,4 cm
r = 7,5 cm
r = 5,6 cm
r = 3,4 cm
r = 1,9 cm
r = 0 cm
r = − 1,9 cm
r = − 3,4 cm
r = − 5,6 cm
r = − 7,5 cm
r = − 9,4 cm

FIG. 17

FIG. 18

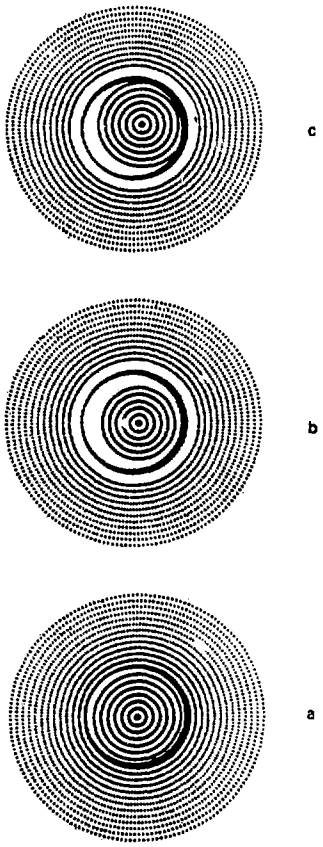

FIG. 19

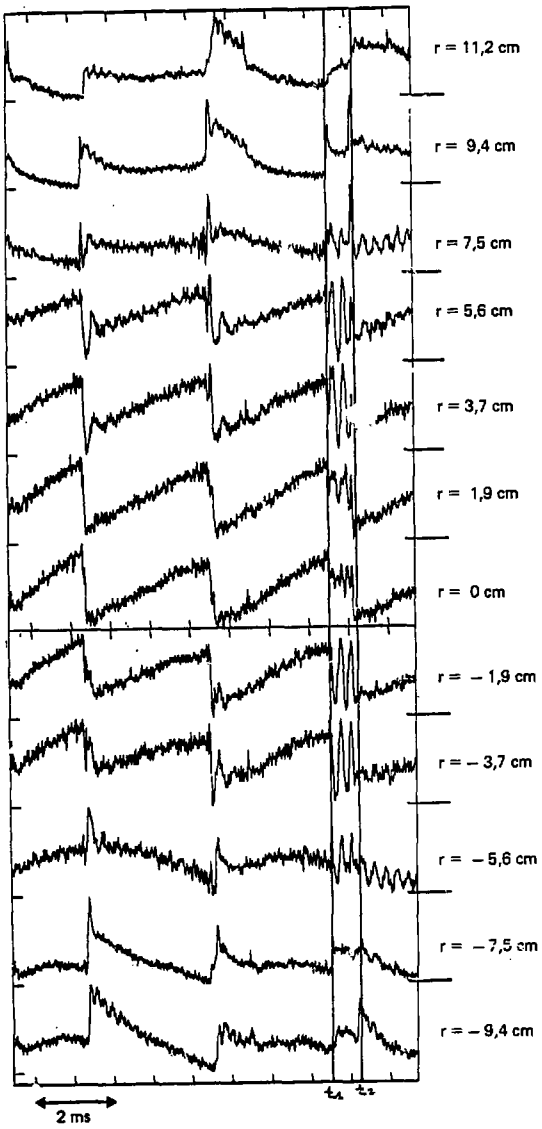
r = 11,2 cm
r = 9,4 cm
r = 7,5 cm
r = 5,6 cm
r = 3,7 cm
r = 1,9 cm
r = 0 cm
r = − 1,9 cm
r = − 3,7 cm
r = − 5,6 cm
r = − 7,5 cm
r = − 9,4 cm
t1
t2
2 ms

FIG. 20